UNIVERSIDADE FEDERAL
DE SANTA CATARINA

Mechanical Engineering Department

EMC410104 - Computational Vibroacoustics

Homework Assignment 1

Professor:
Julio A. Cordioli
Mechanical Engineering
Department

Student:
Lucas Schroeder

August 23, 2021

Contents

1 Introduction

The objective of this assignment is to perform a numerical modal analysis of a beam structure with variable cross-section using two techniques: Rayleigh-Ritz and Finite Element Methods, RRM and FEM, for short. This document is organized as follows: section 1 will present the problem, the parameters and boundary conditions, section 2 will present the energy functions for a beam bending element. section 3 will describe the RRM and how we may use the Lagrange equation to obtain the inertia and stiffness matrices, and show the results obtained with this method, while section 4 will present an extension of the RRM ideas using simpler base functions to determine the inertia and stiffness matrix, and will also show the results. Finally, section 5 will comment on a few challenges and important notes about the codes developed.

The problem consists of a beam structure with variable cross-section that is fixed in the left end, free on the right end, has a gear and two springs mounted as Figure 1 shows. The figure also shows the geometry parameter, such as length and diameters, as well as the weight of the gear. The material were model as linear elastic, with density $\rho = 7700kg$ and Young's modulus $E = 2.1e11Pa$, and the springs stiffness are $k = 10kN/m$ each.

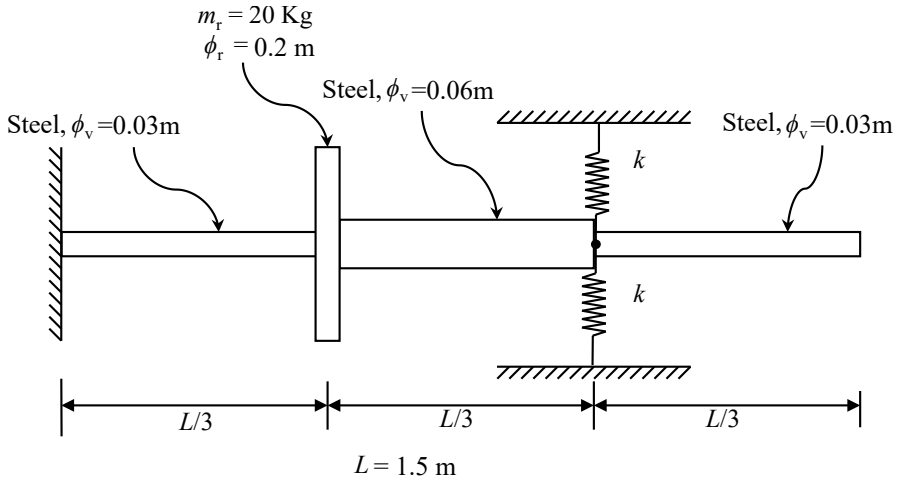

Figure 1: Beam schematics

The goal it to compute the first four natural frequencies and mode shapes using FEM and RRM with different computational settings the will be described in each section.

2 Beam Bending Element Energy Function

It can be shown that the equations of motion for a mechanical system may be derived from its energy function, *i.e.*, the strain and kinetic energy, as well as the virtual work performed by external forces and, possibly, energy dissipation functions. For the purpose of this assignment, we may use an linear elastic model to derive the energy functions of the element shown in Figure 2.

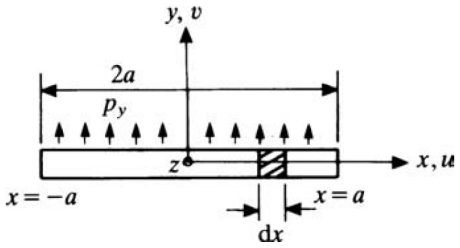

Figure 2: Beam element in local coordinate system. Source: [1]

As shown by Petyt [1], the strain energy of the beam element is

$$U = \frac{1}{2}\int_{-a}^{+a} EI_z \left(\frac{\partial^2 v}{\partial x^2}\right)^2 dx, \tag{1}$$

the kinetic energy of the beam element is

$$T = \frac{1}{2}\int_{-a}^{+a} \rho A \dot{v}^2 dx, \tag{2}$$

and the virtual work in the complete element due to the distributed force p_y is

$$\delta W = \int_{-a}^{+a} p_y \delta v dx. \tag{3}$$

3 Rayleigh-Ritz Method

The Rayleigh-Ritz Method uses a finite series expansion to approximate the solution of the equation of motion, writing the degree-of-freedom (DoF) as linear combination of generalized coordinates $q_j(t)$ and base function $d_j(x)$ as:

$$v(x,t) \approx \sum_{j=1}^{n} d_j(x) q_j(t) = \{d_j(x)\}^T \{q_j(t)\}. \tag{4}$$

By doing this, we are reducing the infinite number of DoF os the original continuous system to a finite amount, n. However, the choice of basis functions are no easy task, because they must satisfy the following conditions [1]:

1. Satisfy the geometric boundary conditions
2. Form a base to $\mathcal{C}^p[0, L]$, the set of p-times continuously differentiable functions on the interval $[0, L]$:
   (a) Must be linearly independent
   (b) Must be p-times continuously differentiable
   (c) The series must converge in the mean (mean square error goes to zero as n goes to infinity)

Choosing the appropriate set of functions $\{d_j(x)\}$, we may substitute Equation 4 in Equation 2 to obtain:

$$T = \frac{1}{2} \{\dot{q}(t)\}^T \left[\int_0^L \rho A \{d(x)\} \{d(x)\}^T dx \right] \{\dot{q}(t)\}, \tag{5}$$

where the term between square brackets is a nxn matrix, called the inertia matrix $[M]$. In the same way, Equation 4 may be substituted in Equation 1 to obtain

$$U = \frac{1}{2} \{q(t)\}^T \left[\int_0^L EI_z \{d''(x)\} \{d''(x)\}^T dx \right] \{q(t)\}, \tag{6}$$

where the term between square brackets is the nxn stiffness matrix $[K]$. Rewriting the equations above as $T = \frac{1}{2} \{\dot{q}(t)\}^T [M] \{\dot{q}(t)\}$ and $U = \frac{1}{2} \{\dot{q}(t)\}^T [K] \{\dot{q}(t)\}$, and recognizing that

$$\left\{ \frac{\mathrm{d}}{\mathrm{d}t} \left(\frac{\partial T}{\partial \dot{q}} \right) \right\} = [M] \{\ddot{q}\} \tag{7}$$

and

$$\left\{\frac{\partial U}{\partial q}\right\} = [K]\{q\}, \tag{8}$$

we may substitute them in Laplace's equation to obtain the equation of motion in the generalized coordinates $\{q_j(t)\}$, to wit:

$$[M]\{\ddot{q}\} + [K]\{q\} = 0 \tag{9}$$

It's important to notice that we are assuming that there is no energy dissipation mechanism in play, and also there is no external forces acting on the beam.

3.1 Inertia and Stiffness Matrices

In the problem at hand, the gear mass and inertia, and the spring stiffness will be treated as lumped parameters. Their effect on $[K]$ and $[M]$ may be easily visualized when we recall that Equation 5 and Equation 6 account for the kinetic energy and strain energy, respectively, of the entire system. Therefore, when $x = L/3$, the integral in Equation 5 assumes the value of

$$[M_{gear}] = m\{d(x = L/3)\}\{d(x = L/3)\}^T + J_z\{d'(x = L/3)\}\{d'(x = L/3)\}^T, \tag{10}$$

and the integral in Equation 6 assumes the value of

$$[K_{springs}] = 2k\{d(x = L/3)\}\{d(x = L/3)\}^T. \tag{11}$$

For the other parts of the beam, the integrals to determine the elements m_{ij} and k_{ij} of the matrices $[M]$ and $[K]$ are straightforward, so the final form of inertia matrix elements is

$$\begin{aligned} m_{ij} = \int_0^{L/3} \rho A_1 d_i(x) d_j(x) dx + \int_{L/3}^{2L/3} \rho A_2 d_i(x) d_j(x) dx + \int_{2L/3}^{L} \rho A_3 d_i(x) d_j(x) dx \\ + m d_i(x = L/3) d_j(x = L/3) + J_z d_i'(x = L/3) d_j'(x = L/3), \end{aligned} \tag{12}$$

and for the stiffness matrix elements have the form

$$k_{ij} = \int_0^{L/3} EI_{z1} d_i''(x) d_j''(x) dx + \int_{L/3}^{2L/3} EI_{z2} d_i''(x) d_j''(x) dx + \int_{2L/3}^{L} EI_{z3} d_i''(x) d_j''(x) dx + 2k d_i(x = L/3) d_j(x = L/3). \quad (13)$$

Notice that $m_{ij} = m_{ji}$ and $k_{ij} = k_{ji}$, that is, both $[K]$ and $[M]$ are symmetric. This is exploited in the code by computing only the superior triangle of each matrix, and then selecting eigenvalue algorithm optimized to real symmetric matrices.

3.2 Eigenvalue Problem

Now that we have the system's matrices we will solve the equation of motion using the modal analysis strategy. We have written the system's response in generalized coordinates using d_j as base, so we may solve the generalized eigenvalue problem $det([K] - \omega_j^2[M])\{A_j\} = 0$ to obtain the natural frequencies and the coordinates of the mode shapes $\{\Phi_j\}$. However, $[A_j]$ is nxn matrix representing the shapes in the $d_j(x)$ base, with n mode shapes. To obtain the real mode shapes we must recall Equation 4 in order to obtain:

$$[\Phi]_{mxn} = [d(x)]^T_{mxn}[A]_{nxn}, \quad (14)$$

where m is the number of points in the discretized domain (beam length).

3.3 Results

The base function used were suggested in the assignment statement, based on the mode shapes of a constant cross-section homogeneous cantilever and have the following form:

$$d_j(x) = sin(\eta_j x) - sinh(\eta_j x) + D_j(cos(\eta_j x) - cosh(\eta_j x)), \quad (15)$$

where

$$D_j = \frac{cos(\eta_j L) + cosh(\eta_j L)}{sin(\eta_j L) - sinh(\eta_j L)}, \quad (16)$$

and

$$\eta_j \approx \begin{cases} 1.875/L, & j = 1 \\ \frac{(j-0.5)\pi}{L}, & j > 1 \end{cases} \tag{17}$$

Those base functions have the shapes plotted in Figure 3.

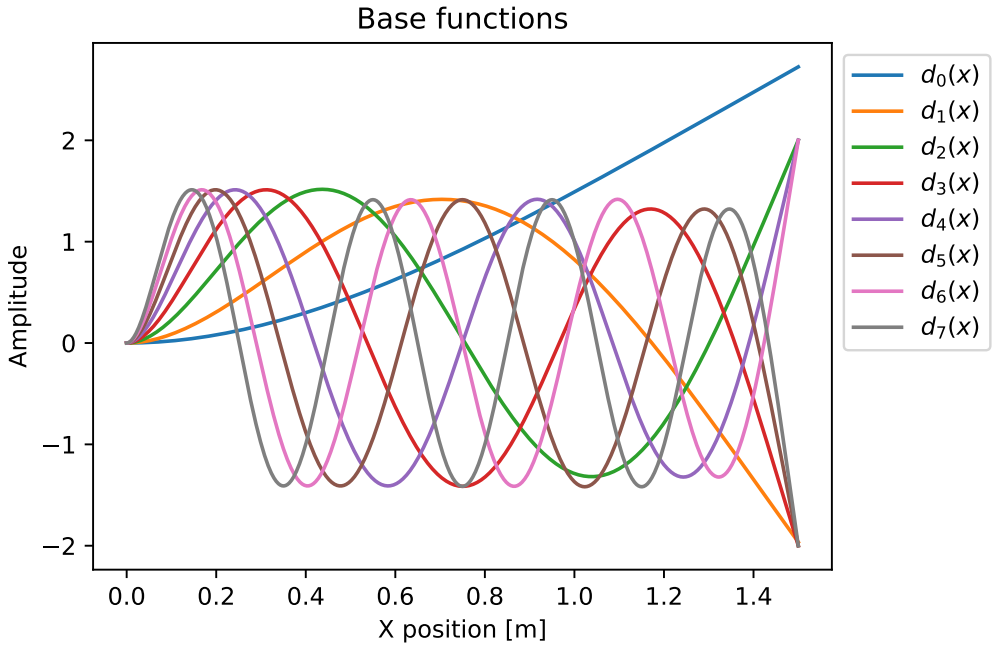

Figure 3: Base functions plot

To solve the generalized eigenvalue problem we used the eigh function of the Scipy module, which is optimized to solve eigenvalues of dense real symmetric matrices. The results of natural frequencies for different number of base functions (4, 8, 12 and 16) are shown in Table 1. However, the convergence of natural frequencies are better visualized in Figure 4, where its evident that for the first two modes, a few elements are sufficient, but for for modes three and four, a lager number of elements makes a much bigger difference.

Finally, the mode shapes obtained are shown in Figure 5, where the same trend is visible: the first two modes are well defined by a few base functions, but higher modes need more base functions to be reasonably represented.

Table 1: First four natural frequencies, in Hz, from different number of base functions, n.

	f_1	f_2	f_3	f_4
n=4	9.85	61.39	218.68	506.06
n=8	9.73	51.02	147.71	449.84
n=12	9.71	48.97	136.75	446.54
n=16	9.70	48.07	133.79	445.15

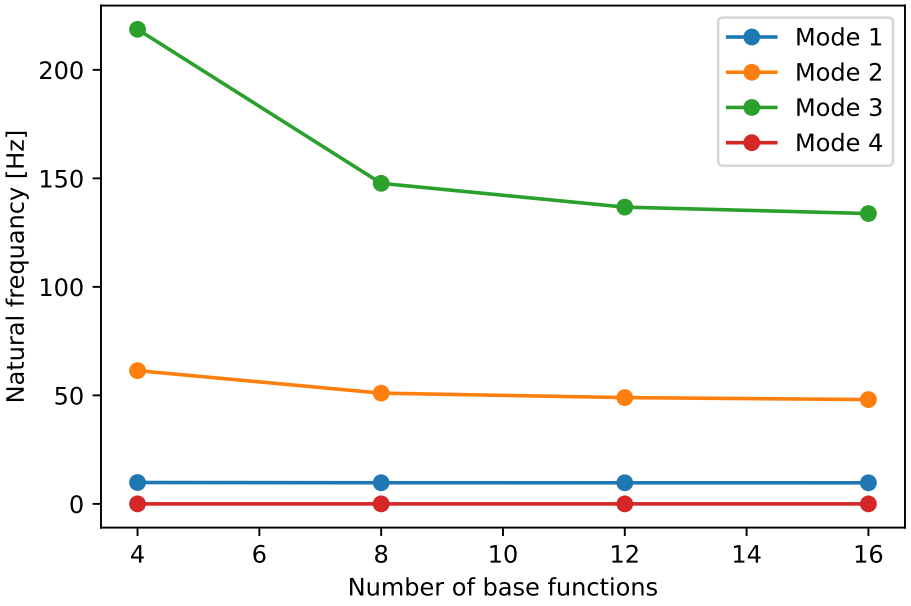

Figure 4: Natural frequencies convergence, RRM

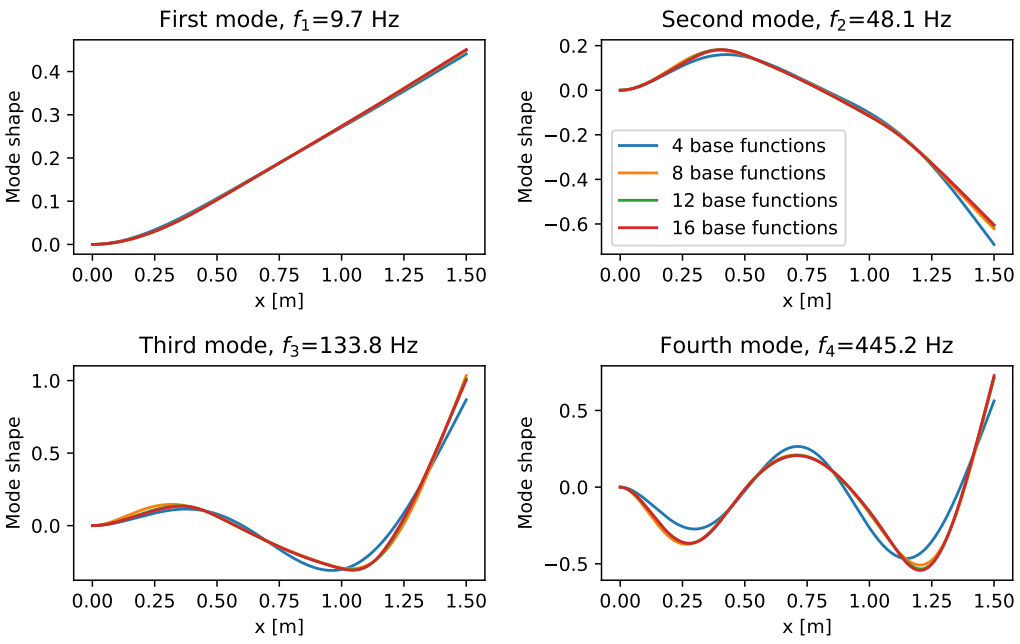

Figure 5: Mode shapes obtained via RRM

4 Finite Element Method

This chapter will present the Finite Element Method, which solves the main problem with RRM: finding adequate base functions that complies with all the requirements. This is done using the concept of elements and shape functions: we can represent a structure using a finite number of elements, and represent the displacements inside each element by an arbitrary shape function (that must satisfy a few conditions) that have its coefficients defined by the displacements and rotations of the elements nodes.

4.1 Element matrices

For the problem at hand, we will use the beam bending element presented at section 2, and a cubic shape function:

$$\varphi = \alpha_0 + \alpha_1\xi + \alpha_2\xi^2 + \alpha_3\xi^3 \tag{18}$$

This function have four degrees of freedom (α_i) and have and important feature: at each node, we may force it to have a unit value for a given DoF (displacement or rotation of each beam node), while having zero for the others at each node. In this way, we write the vertical displacement of the beam element as:

$$v(\xi) = \alpha_0 + \alpha_1\xi + \alpha_2\xi^2 + \alpha_3\xi^3 = \begin{Bmatrix}1 & \xi & \xi^2 & \xi^3\end{Bmatrix} \begin{Bmatrix}\alpha_0 \\ \alpha_1 \\ \alpha_2 \\ \alpha_3\end{Bmatrix} = \{P(\xi)\}^T\{\alpha\} \tag{19}$$

The goal is to characterize the continuous displacement field inside the element using only the displacement and rotation at each node. To do this, we evaluate the equation above at both nodes, where $\xi = \pm 1$, and we do the same for the nodes rotation $\theta_z(x) = \frac{\partial v(x)}{\partial x}$, and the four equations may be written in the matrix form as:

$$\begin{Bmatrix}v_1 \\ a\theta_{z1} \\ v_2 \\ a\theta_{z2}\end{Bmatrix} = \begin{bmatrix}1 & -1 & 1 & -1 \\ 0 & 1 & -2 & 3 \\ 1 & 1 & 1 & 1 \\ 0 & 1 & 2 & 3\end{bmatrix} \begin{Bmatrix}\alpha_0 \\ \alpha_1 \\ \alpha_2 \\ \alpha_3\end{Bmatrix} \tag{20}$$

Which can be solved for α and substituted into Equation 19 yielding:

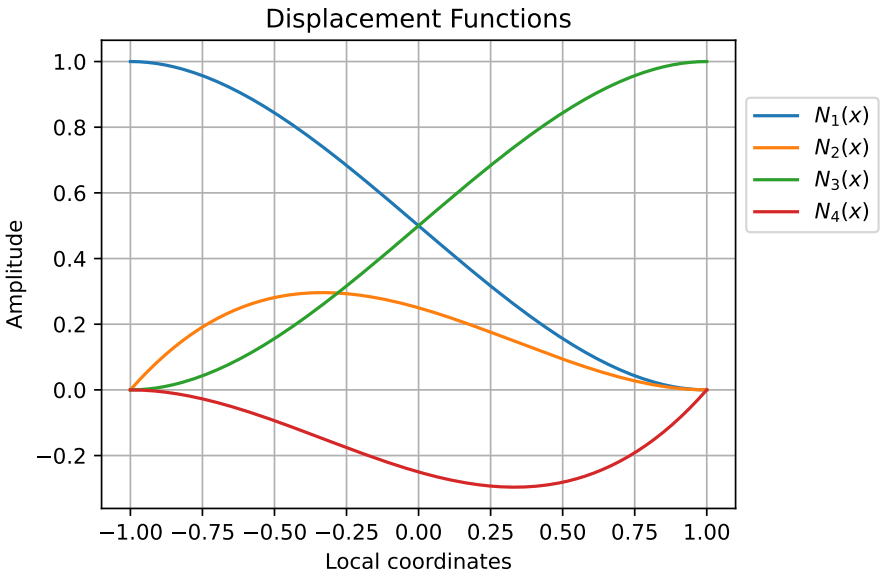

Figure 6: Beam element displacement functions

$$v(\xi) = \begin{Bmatrix} N_1 = \frac{1}{4}(2 - 3\xi + \xi^3) \\ aN_2 = a\frac{1}{4}(1 - \xi - \xi^2 + \xi^3) \\ N_3 = \frac{1}{4}(2 + 3\xi - \xi^3) \\ aN_4 = a\frac{1}{4}(-1 - \xi + \xi^2 + \xi^3) \end{Bmatrix}^T \begin{Bmatrix} v_1 \\ \theta_{z1} \\ v_2 \\ \theta_{z2} \end{Bmatrix} = \{N(\xi)\}^T \{v\}_e = \sum_{i=1}^{4} u_i N_i(\xi). \tag{21}$$

The element displacement functions have the curves plotted in Figure 6. Here we can see that N_1 have a unitary displacement and zero rotation at the first node, and zero displacement and rotation at the second node. N_2 has unitary rotation at node one, but the other three DoF are zero, and the same characteristic apply to the other functions.

This means that we can use only four DoF to represent $v(x)$ as a linear combination of the shape functions $\{N(\xi)\}$ (column vector representation) with weight given by the response $\{u\} = \begin{Bmatrix} v_1 & a\theta_{z1} & v_2 & a\theta_{z2} \end{Bmatrix}^T$ at the two nodes. The next step is to calculate the kinetic and strain energy of the element substituting Equation 21 into Equation 2 and Equation 1, to obtain the mass ($[m_e]$) and stiffness ($[k_e]$) matrix of the element in the generalized coordinates $\{v_e\}$. For the mass we obtain:

$$T_e = \frac{1}{2}\{\dot{v}\}_e^T \rho A a \int_{-1}^{1} \{N(\xi)\}\{N(\xi)\}^T d\xi \{\dot{v}\}_e, \tag{22}$$

where

$$[m_e] = \rho A a \int_{-1}^{1} \{N(\xi)\}\{N(\xi)\}^T d\xi = \rho A a \begin{bmatrix} 78 & 22a & 27 & -13a \\ 22a & 8a^2 & 13a & -6a^2 \\ 27 & 13a & 78 & -22a \\ -13a & -6a^2 & -22a & 8a^2 \end{bmatrix}. \tag{23}$$

For the element strain we get

$$U_e = \frac{1}{2}\{v\}_e^T \frac{EI_z}{a^3} \int_{-1}^{1} \{N''(\xi)\}\{N''(\xi)\}^T d\xi \{v\}_e, \tag{24}$$

where

$$[k_e] = \frac{EI_z}{a^3} \int_{-1}^{1} \{N''(\xi)\}\{N''(\xi)\}^T d\xi = \frac{EI_z}{a^3} \begin{bmatrix} 3 & 3a & -3 & 3a \\ 3a & 4a^2 & -3a & 2a^2 \\ -3 & -3a & 3 & -3a \\ 3a & 2a^2 & -3a & 4a^2 \end{bmatrix}. \tag{25}$$

We may also substitute Equation 21 into Equation 3 to obtain the vector of element forces:

$$\delta W_e = \{\delta v\}_e^T a \int_{-1}^{1} p_y \{N(\xi)\} d\xi \tag{26}$$

where

$$\{f\}_e = a \int_{-1}^{1} p_y \{N(\xi)\} d\xi = p_y^e \frac{a}{3} \begin{Bmatrix} 3 \\ a \\ 3 \\ -a \end{Bmatrix} \tag{27}$$

4.2 Global matrix assembly

Now that we have the strain and kinetic energy of the element written as functions of generalized coordinates $\{v\}_e$ and its matrices, we substitute them in Lagrange's equation to obtain the element's equation of motion.

$$[m_e]\{\ddot{v}\}_e + [k_e]\{v\}_e = \{f\}_e. \tag{28}$$

The construction of the global system of equation are based in the dynamic equilibrium of each element as well as the dynamic equilibrium of each node of the entire system. In this way, we observe that, apart from the first and last global nodes, each node belongs to two elements, which means that there will be two equations for each DoF of $\{v\}_e$. Furthermore, there are no external forces and the internal forces sum to zero, that is, the only forces acting on each node form pairs action-reaction, apart from the first node, which is fixed and have the force and moment of the wall action on it. Therefore, when we assemble the global matrices that represent the system of equations of motion of every DoF of the system, we end up with a system of nxn equations, where n is the total number of DoF, with force the vector all elements equal to zero, but the first two. However, we already know the response of the first two DoF: they are zero, by hypothesis, and we can safely remove this equations from our system. To do this, we simply remove the rows and columns of the global mass and stiffness matrices to be able to solve the system.

To account for the lumped parameters of the gear mass and the springs stiffness, we observe that we can write individual equations of motion for the DoF they influence, and sum its contribution in the appropriate row and columns of the global $[K]$ and $[M]$ matrices.

4.3 Eigenvalue Problem

As in the previous chapter, now that we have the system's matrices we will solve the equation of motion using the modal analysis strategy. We have written the system's response in generalized coordinates using $\{v\}$, which contains the displacement and rotation of every node of the system, so we may solve the generalized eigenvalue problem $det([K] - \omega_j^2[M])\{A_j\} = 0$ to obtain the natural frequencies and the coordinates of the mode shapes $\{\Phi_j\}$.

4.4 Results

To solve the generalized eigenvalue problem we used the eigsh function of the Scipy module, which is optimized to find the first k eigenvalues and eigenvectors of a real symmetric square matrix.

The process of discrediting and assembly of matrices was done for three different number of elements: 9, 12, and 72 beam elements. The results for natural frequencies are shown in Table 2, and the mesh convergence study plot is shown in Figure 7.

To plot the mode shape, we have two options:

1. Simply plot the coordinate of the DoF associated with the vertical displacement, or

Table 2: First four natural frequencies, in Hz, from different number of elements, n.

	f_1	f_2	f_3	f_4
n=9	9.67	44.26	124.22	441.03
n=18	9.67	44.26	124.21	440.37
n=72	9.67	44.26	124.20	440.32

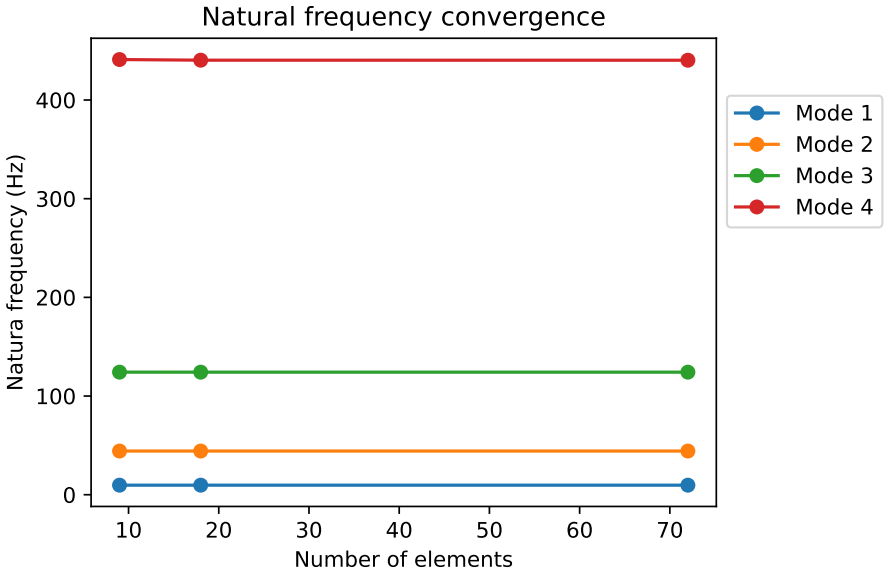

Figure 7: Natural frequencies convergence plot

2. Use the computed element coordinate $\{v\}$ in Equation 21 to find a more complete description of the displacement field $v(x)$.

For comparison, Figure 8 show the results obtained with both approaches. Furthermore, Figure 9 show the results of the first three mode shapes with all discretization levels, and Figure 10 show the same, but interpolating the space using the shape functions defined in Equation 21.

That problem was a good example for the power of FE method, with only 9 beam elements we were able to compute the first four natural frequencies with 0.16% accuracy, and unrecognizable differences in mode shapes.

Finally, we present a comparison of the results obtained with FEM and RRM. Table 3 show the first four natural frequencies obtained using RRM with 16 base functions, and using FEM with 72 beam elements, where we can see differences smaller than

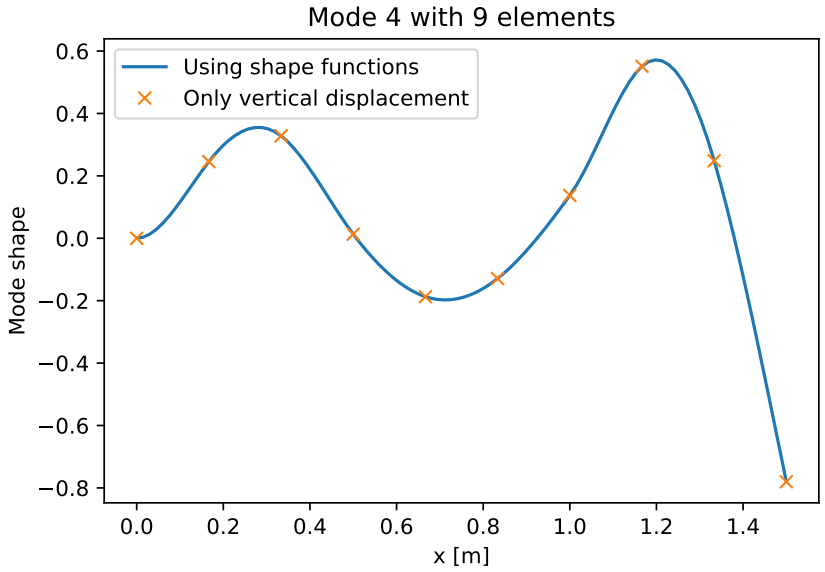

Figure 8: Mode shapes using the complete shape function vs. only the vertical displacement

9%. For comparison, the first four mode shapes are shown in Figure 11, where we can see an almost perfect match. Another important aspect of this results is the computational cost, and RRM has two main disadvantages: (1) the matrices are more expensive to build, since they are full. Even though they are smaller, it took around 15 seconds, versus 0.1 second of the FEM matrices. (2) The generalized eigenvalue problem of FEM is better optimized, since the matrices are sparse.

Table 3: First four natural frequencies, in Hz, with RRM and FEM

	f_1	f_2	f_3	f_4
RRM	9.70	48.07	133.79	445.15
FEM	9.67	44.26	124.20	440.32

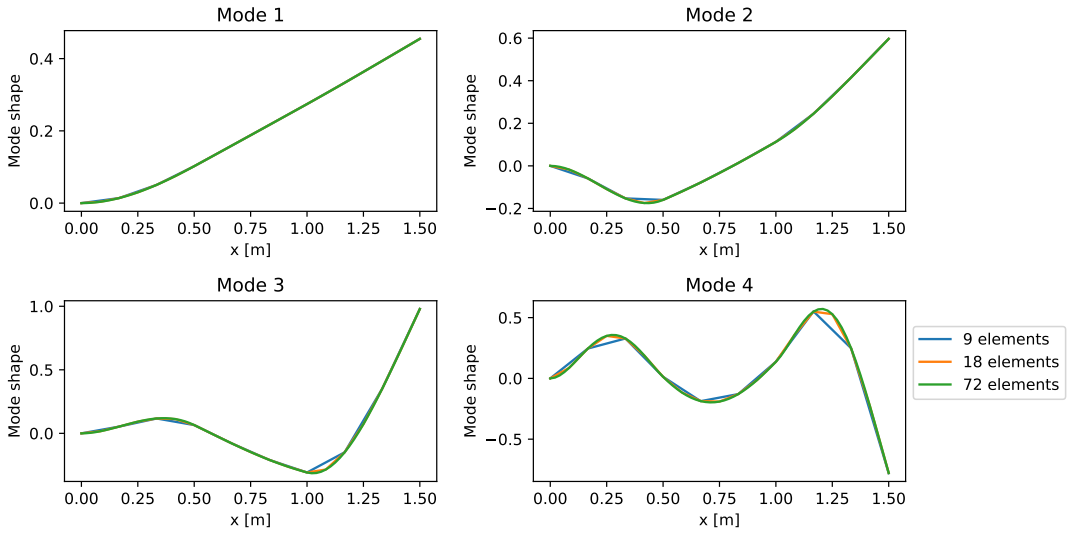

Figure 9: Mode shapes using only the vertical displacement coordinates.

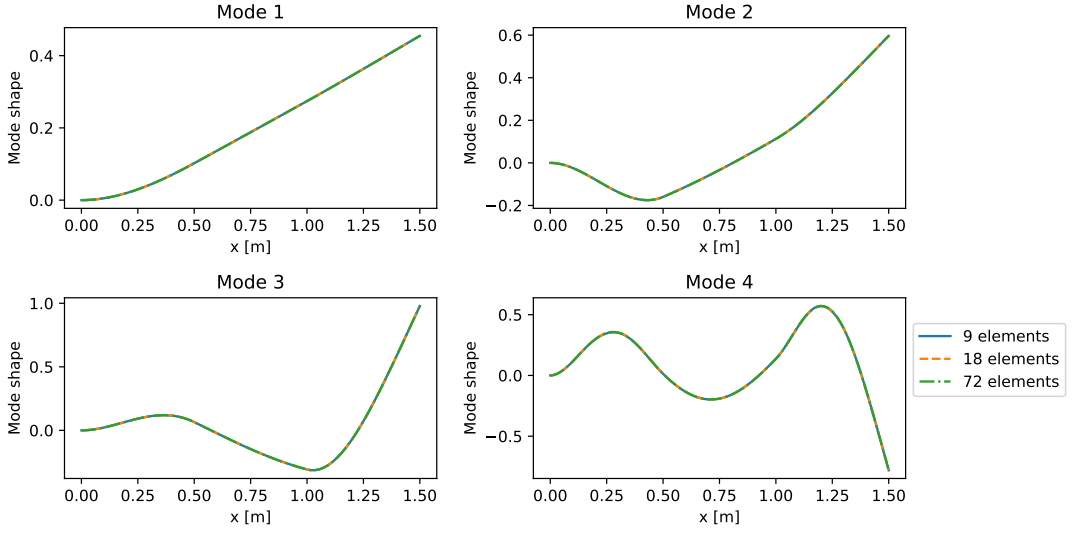

Figure 10: Mode shapes using shape functions.

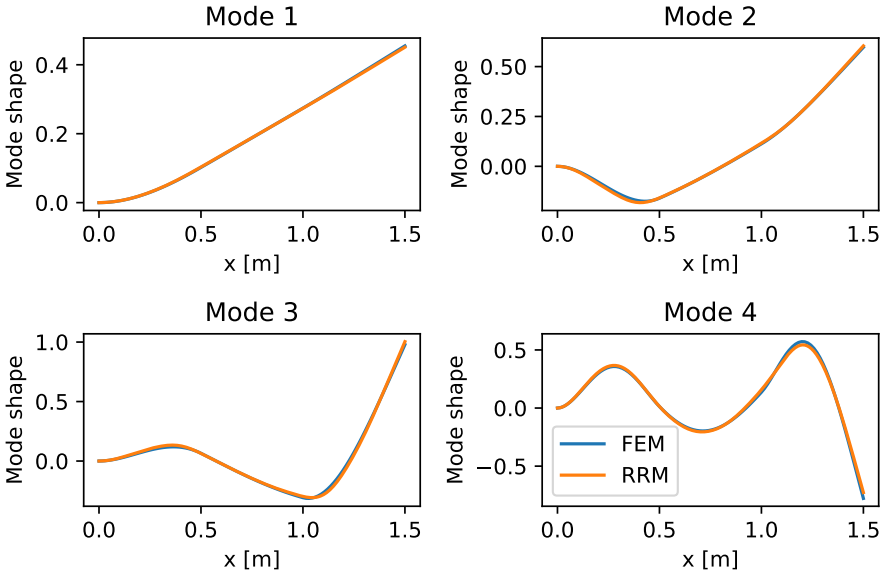

Figure 11: Mode shapes obtained with FEM and RRM.

5 Final remarks

The codes of this work were developed in Python using NumPy, SciPy, Pandas, and Matplotlib free and open source modules. Although they form a wonderful and powerful set of tools, a few challenges had to be overcome.

5.1 Numerical instability

When solving the problem using RRM, the base functions defined in Equation 15 presented problems when calculated for $j > 10$ and $x > 1.0$. The symptoms are shown in Figure 12, where the computed values of the function are wrong from around $x = 1$

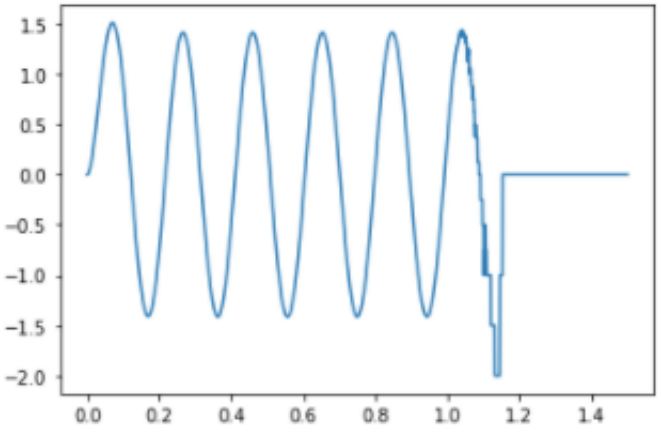

Figure 12: d_j base function for $j = 10$

The problem was due to numerical instabilities when performing the sum of a very large number ($sinh(\eta_j x)$) with a much smaller number ($sin(\eta_j x)$). As discussed in this StackOverflow question, when to float numbers are summed, there is lost in numerical precision, and this lost is very significative when the two number have very different orders of magnitude. To overcome this problem, the expression for $d_j(x)$ were rewritten using the hyperbolic sine and cosine definitions as

$$d_j = sin(\eta_j x) + D_j cos(\eta_j x) - \frac{1}{2}((D_j - 1)e^{-\eta_j x} + (D_j + 1)e^{\eta_j x})), \tag{29}$$

therefore, avoiding the numerical summation of numbers with very large difference in orders of magnitude.

References

[1] Maurice Petyt. *Introduction to Finite Element Vibration Analysis*. Cambridge University Press, August 2010. ISBN 978-1-139-49006-1.